# Supplemental Information

# Closed-Loop Measurements

# of Iso-Response Stimuli Reveal Dynamic

# Nonlinear Stimulus Integration in the Retina

Daniel Bölinger and Tim Gollisch

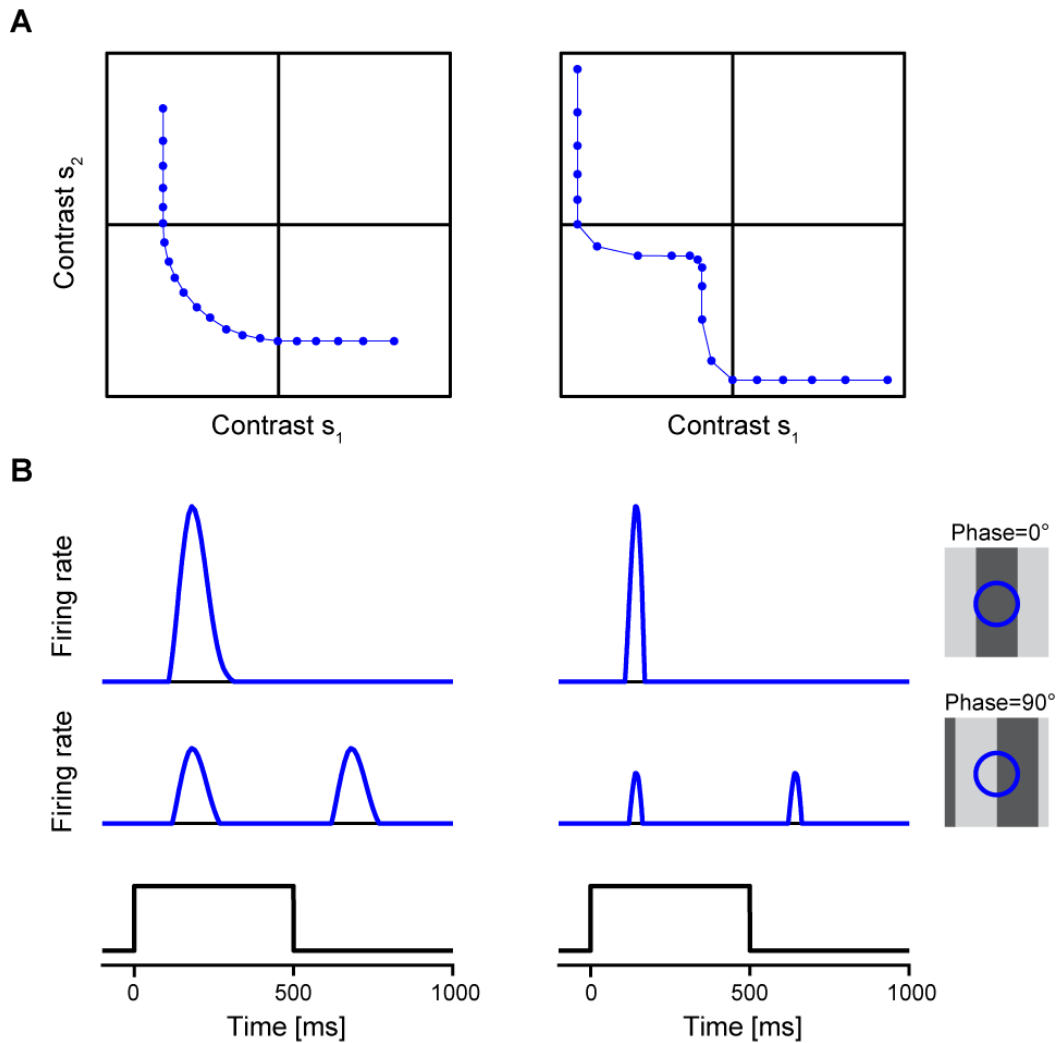# Supplemental Figure S1

**A**



**B**



**Figure S1 (related to Figure 7). Simulated responses of cells with convex and non-convex iso-response curves to contrast-reversing grating stimuli**

(A) Iso-rate curves of two simulated ganglion cells, one with convex iso-rate curve (left), obtained by setting the amacrine cell signal in the model of Figure 7C to zero, and one with non-convex iso-rate curve (right), obtained from the full model of homogeneity detectors.

(B) Responses of the two simulated ganglion cells to contrast-reversing gratings. Gratings had a stripe width of exactly the receptive field diameter. As shown schematically on the right, the receptive field was either aligned to lie completely on a single grating stripe (phase=0°, top) or to straddle the border of two stripes (phase=90°, middle). The time course of grating reversals is shown on the bottom. For each simulated ganglion cell, responses are shown as peri-stimulus time histograms, normalized to the peak firing rate at phase=0°. Both cells show similar response patterns, characteristic of Y-type ganglion cells, with pronounced response peaks to both reversals of the grating at 90° spatial phase.

# Supplemental Experimental Procedures

### Electrophysiology

Retinas were obtained from dark-adapted adult axolotl salamanders (Ambystoma mexicanum; pigmented wild type) of either sex. After enucleation of the eyes, retinas were isolated from the eye cup and cut in half. One retina half was placed ganglion-cell-side-down on a planar multi-electrode array (Multichannel Systems, 60 channels, 10-μm electrode diameter, 100-μm spacing) for extracellular recording, while the other retina pieces were stored in oxygenated Ringer's solution (110 mM NaCl, 2.5 mM KCl, 1.6 mM $MgCl_2$, 1.0 mM $CaCl_2$, 22 mM $NaHCO_3$, 10 mM D-glucose, equilibrated with 95% $O_2$ and 5% $CO_2$) for later recording. The preparation was performed with infrared illumination under a microscope equipped with night-vision goggles. During recordings, retinas were continuously perfused with the Ringer's solution at room temperature (20°C-22°C). The measured voltage signals were amplified, band-pass filtered between 200 Hz and 5 kHz, and digitized at a sampling frequency of 25 kHz.

For experiments with a pharmacological block of inhibition (Figure 7), we added strychnine (5 μM), picrotoxin (150 μM) and bicuculline (20 μM) to the Ringer's solution and waited 20 minutes before resuming measurements. We then first re-determined the threshold criterion of spike detection for the online analysis and verified that spikes could still be reliably detected.

### Visual stimulation

To visually stimulate the retina, the screen of a gamma-corrected cathode ray tube monitor was focused with standard optics from above onto the photoreceptor layer. The projection of the screen covered the recorded piece of retina. Pixel resolution on the retina was approximately 6 μm. The stimulus screen was updated with a frame rate of 100 Hz and controlled through custom-made software, based on Visual C++ and OpenGL. Stimuli were presented on a gray background in the photopic range of either 5.1 mW/m² or 9.3 mW/m² with no difference in results. We estimated isomerization rates based on the measured spectrum of the light source and the photopigment spectral sensitivities (Makino et al., 1991) as well as the collecting areas (Perry and McNaughton, 1991; Yang and Wu, 1997) of rods and cones in the closely related tiger salamander (Ambystoma tigrinum). For the three major photoreceptor types (red-sensitive rod, L cone, S cone), we obtained the following values in isomerizations per receptor cell per second for the two different background light intensities: $2.5 \times 10^5$ (rod), $4.9 \times 10^3$ (L cone), $3.2 \times 10^3$ (S cone) and $4.4 \times 10^5$ (rod), $8.8 \times 10^3$ (L cone), $5.7 \times 10^3$ (S cone), respectively.

**Online search algorithms in closed-loop experiments**

**a) Determination of receptive field**

First, the receptive field midpoint was determined as the crossing point of two orthogonal midlines of the receptive field. Each of these midlines was found in the following way: We separated the available stimulation area by a straight separation line into two regions and presented alternating black–white stimulation at 1 Hz for 6 sec first in one region and subsequently in the other region and calculated the difference in spike count for the two regions. We then used a simple automated search algorithm to find the separation line that yielded zero spike count difference. This search algorithm consisted of two phases. In phase 1, the separation line was shifted after each pair of stimuli by 40 pixels towards the side for which stimulation yielded more spikes. This was repeated until the first "sign change" was observed, that is, until that side yielded more spikes that had previously yielded less. In the following phase 2, 15 additional measurements were performed. After each measurement, the separation line was again shifted in the direction where more spikes were observed, but the number of pixels of this shift was chosen randomly from a uniform distribution between 1 and 20 pixels. The final midline of the receptive field was then determined by a linear fit of the spike count differences versus position of the separation line for the 15 measurements of phase 2.

Subsequently, in order to determine the diameter of the receptive field center, a blinking spot was presented, centered on the obtained receptive field midpoint. The spot alternated between black and white at 1 Hz for 6 sec, and the spot diameter was successively increased from 10 to 200 pixels in steps of 10 pixels. The diameter that elicited the maximum spike number was used as the diameter of the receptive field center.

**b) Iso-response measurements**

The stimuli applied in the measurements of iso-response curves consisted of a circular spot, centered at the cell's receptive field midpoint and with a diameter that corresponded to the estimated diameter of the receptive field center (Figure 1D). The spot was divided into two halves, and each stimulus consisted of a pair of contrast values $(s_1, s_2)$, denoting the contrasts that were displayed in each of the two halves. The two contrast values span the two-dimensional stimulus space, in which iso-response curves were analyzed (Figure 2A). Individual stimuli were presented either for 200 ms or for 500 ms, and spike counts were determined over 300 ms or 500 ms, respectively, with no differences in results. Typically, a single stimulus presentation was used for every stimulus; in some trial experiments, each stimulus was repeated twice and responses were averaged, again with no effect on results.

In the experiments with the pre-depression stimulus (Figure 6), each stimulus presentation used for the iso-response measurement was preceded by a brief dark flash (contrast = -40%) on one half of the receptive field. For experiments with 200-ms stimulation in the control case, the pre-depression stimulus lasted for 200 ms and was followed by a 300-ms pause; for experiments with 500-ms stimulation, pre-depression stimulus and pause each lasted 500 ms. Note that to measure the response in these experiments, only spikes from the actual iso-response stimulus were taken into account; spikes resulting from the pre-depression stimulus were not considered.

Individual line searches for iso-response stimuli operated along a radial direction in the stimulus space. The direction was determined by fixing a certain angle in stimulus space, which determines the relative strength of $s_1$ and $s_2$. Along this direction, a search algorithm (see below) was applied to find that radius $r = \sqrt{s_1^2 + s_2^2}$ that corresponded to the predefined response. Typically, we interleaved measurements along multiple search directions in a randomized fashion in order to minimize adaptation effects. In some experiments, the measurements were performed one search direction after another with no differences in results. In the following, we describe the line search along an individual search direction for a predefined spike count. Searches for predefined latencies were performed analogously.

The search algorithm proceeded similarly to the online estimation of the receptive field center spot. The search consisted of two phases. In phase 1, the radius $r$ was increased step-by-step, starting from contrast zero, until the measured spike count was larger than the predefined response. The step size was 10% contrast for the larger of the two contrast values, while the smaller contrast changed correspondingly so that the fixed ratio of the two contrast values was preserved. In the subsequent phase 2, 15 further measurements were performed, and the contrast adjustment before each stimulus presentation was chosen randomly from a uniform distribution between 0 and 10%. Again, the larger of the two contrast values was adjusted by this amount while the smaller contrast value was changed accordingly so that the fixed ratio was preserved. The adjustment was used as a contrast increase if the previous spike count had been too small and as a decrease if it had been too large. If the response had been the exact target response, it was chosen at random whether the next step was an increase or decrease. Finally, the data from search phase 2 were fitted by a linear function (iso-rate curves, e.g. Figure 2C) or an exponential function (iso-latency curves, e.g. Figure 2D):

Iso-rate curves: $\quad\quad Rate = Rate_{\text{target}} + b(r - r_0)$

Iso-latency curves: $\quad Lat = (Lat_{\text{target}} - b) \cdot \exp(-(r - r_0)/s) + b$

The fit parameters $r_0$ and $b$ (and $s$ in the case of the iso-latency curve) were adjusted according to a least-squares criterion. The curve fit yielded the radius $r_0$ that corresponded to the target response ($Rate_{\text{target}}$ or $Lat_{\text{target}}$). Error bars of the iso-response stimuli represent 95%

confidence intervals of the fit parameter $r_0$. If the target response could not be reached within the available contrast range, the measured data were extrapolated. Such data points are marked in the iso-response plots by dashed lines connecting these points to their neighboring data points.


**Form factors**

We calculated form factors of the iso-response curves to quantify the extent and type of nonlinearity of the curves (Figures 3G-3I). The form factor compares the shape of the curve to the linear prediction, defined by the line between the two intersection points of the curve with the axes. It is larger or smaller than unity depending on whether the iso-response curve is convex or non-convex, respectively. The form factor was obtained in the following way. We first estimated the radius $r(\phi)$ for different polar angles $\phi$ by averaging the radius of all data points (typically three) with polar angles between $\phi - 10°$ and $\phi + 10°$. For the lower left diagonal, which corresponds to homogeneous dark stimulation, we obtained $r(225°)$, and for the negative x axis and negative y axis, we obtained $r(180°)$ and $r(270°)$, respectively. The two latter values can be used to derive the linear prediction for the radius along the lower left diagonal, $r_{pred}(225°)$:

$$r_{pred}\left(225°\right) = \sqrt{2}\,\frac{r\left(180°\right)r(270°)}{r\left(180°\right)+r(270°)} \qquad (1)$$

The form factor is then calculated as the ratio $r(225°)/r_{pred}(225°)$. In some cases, multiple iso-rate or iso-latency curves of the same cell were measured. The values of Figure 3 then report the average form factors.


**Slope of iso-rate curves for assessment of rectification**

To characterize the cells' rectification (Figure 4C), we calculated the average slope of each iso-rate curve in the regions where one contrast component was negative and the other positive. To do so, the data points in the quadrant defined by $s_1 < 0$ and $s_2 \geq 0$ were fitted according to the linear regression model $s_1 = m_a \cdot \left(-s_2\right) + b_a$, and data points in the quadrant defined by $s_1 \geq 0$ and $s_2 < 0$ were fitted by $s_2 = m_b \cdot (-s_1) + b_b$. The slope value that characterized the rectification of the iso-response curve was then obtained as the average of the fit parameters $m_a$ and $m_b$. With the applied sign convention, a slope of zero corresponds to perfect half-wave rectification, whereas a slope of unity means no rectification, i.e., linear integration of $s_1$ and $s_2$.

**Modeling the subunit nonlinearity**

To obtain the nonlinearities for the subunit model (insets of Figures 3A-3C), we fitted individual iso-response curves with a curve of the form

$$1 = \frac{1}{c_1^k} N(s_1) + \frac{1}{c_2^k} N(s_2).$$
(2)

Here, $N(\cdot)$ is the subunit nonlinearity, parameterized as

$$N(s_i) = \begin{cases} m(s_i - \vartheta), & s_i < \vartheta \\ (s_i - \vartheta)^k, & s_i \geq \vartheta \end{cases}.$$
(3)

The variables $m, k, \vartheta$ denote the free parameters of the nonlinearity, and $c_1$ and $c_2$ are scaling parameters that set the sensitivity along each of the axes in the two-dimensional stimulus space. $\vartheta$ denotes a threshold value. For contrast values $s_i$ below $\vartheta$, the nonlinearity is described by a potentially incomplete rectification (complete rectification is obtained for $m = 0$); for larger contrast values, the nonlinearity follows a simple power law, where $k = 2$ corresponds to the quadratic case.

The parameter values were obtained by a standard maximum-likelihood fit. To compute the likelihood, the model prediction for the radius $r = \sqrt{s_1^2 + s_2^2}$ was calculated for each direction in stimulus space for which an iso-response stimulus $(s_1, s_2)$ had been measured. The prediction was obtained by solving the above implicit Eq. (2) of the iso-response curve. The probability of each experimentally measured radius $r$ was then calculated by assuming that the data follow a Gaussian distribution with mean value given by the model prediction and standard deviation given by the experimental measurement error of $r$.

**Modeling the effect of subunit size**

To investigate the effect of subunit size on iso-response curves under stimulation with different stimuli arranged in a checkerboard fashion (Figure 4), we set up a subunit model of a ganglion cell. The ganglion cell's receptive field of 600 µm diameter was assembled by smaller circular subunits. The subunit midpoints were positioned on a rectangular grid so that neighboring subunits touched each other without overlap. For simplicity, we did not consider the time course of the activation and only computed a single activation level for each stimulus by averaging stimulus contrast over the subunit's region. The obtained linear subunit activation $b$ was then transformed by the nonlinearity

$$N(b) = \begin{cases} m \cdot b, & b < 0 \\ m \cdot b + b^2, & b \geq 0 \end{cases}.$$
(4)

This nonlinearity models a rectifying quadratic signal transmission with incomplete rectification. The factor m=0.3 was chosen to approximately reproduce the baseline of rectification that was found experimentally when using the control stimuli, which divided the receptive field into two halves of semicircular shape.

The ganglion cell response was calculated as a weighted sum of all nonlinearly transformed subunit signals. The weights of the subunits followed a Gaussian curve, centered on the receptive field with a standard deviation of 100 µm.

We then used this model to calculate the response to the stimulus with contrast values $s_1 = 1$ and $s_2 = 0$. Afterwards we applied a simple search algorithm to find the stimulus yielding the same response along the direction defined by $s_2 = -s_1 / 2 < 0$. The two obtained iso-response stimuli allowed us to calculate the slope of the iso-response curve in the quadrant where $s_1$ is positive and $s_2$ is negative in the same way as for the experimental data.

Since in the experiments the alignment of the subunits with the stimulus is not known and unlikely to be the same for different cells, we varied the alignment of the subunit grid in the simulations by repeating the computations of iso-response stimuli 200 times, each time with a different random shift of the subunit grid. For each simulation, the weights of the subunits were updated according to the new distance from the receptive field midpoint. The slope values reported in Figure 4C were then obtained as averages over all simulated alignments.


**Modeling homogeneity detectors with local inhibitory circuitry**

To simulate iso-response curves according to the circuit of Figure 7C, we set up a computational model consisting of a homogeneity detector ganglion cell with two independent subunits. Each subunit $i$ was composed of an excitatory bipolar cell and an inhibitory amacrine cell. The bipolar cell input was modeled via a scalar intensity function that steps from 0 (gray) to $s_i$ (positive values: brightening; negative values: darkening).

To determine the bipolar cell activation, the stimulus was convolved with a biphasic temporal Off-type filter. Because the filter was biphasic, a dark stimulus led to a transient bipolar cell excitation. The bipolar cell output $B_i(t)$ was determined by passing this activation through a threshold-quadratic nonlinearity. This output signal served as excitatory input to both the ganglion cell and the amacrine cell.

To obtain the amacrine cell activation $a_i$, the input received from the bipolar cell was low-pass filtered. The low-pass filtering accounts for the temporal delay and was modeled by a first-order differential equation with time constant $\tau = 20\,ms$: $da_i / dt(t) = (B_i(t) - a_i(t)) / \tau$, which can be regarded as a simple model of synaptic transmission. The amacrine cell activation was

calculated iteratively in discrete time steps of $\Delta t = 0.1\,\mathrm{ms}$. To obtain the output of the amacrine cell $A_i(t)$, the activation $a_i$ was transformed by another threshold-quadratic nonlinearity with subsequent scaling to set the relative strength of the inhibition: $A_i(t) = |a_i(t)|_+^2 / 15$.

The input to the ganglion cell was given by summing excitatory and inhibitory signals:

$g(t) = B_1(t) - A_1(t) + B_2(t) - A_2(t)$. Note that identical results were obtained when inhibition was modeled as acting presynaptically on the bipolar cell terminals by including an additional rectification of the terms $B_i(t) - A_i(t)$ in the above equation. The spiking response of the homogeneity detector was modeled by a simple threshold operation with threshold $\vartheta = 6$ and appropriate scaling to obtain firing rates in the physiological range. Thus, we defined the homogeneity detector's firing rate $G(t)$ in Hertz as $G(t) = |g(t) - \vartheta| \cdot 20$.

The first-spike latency was defined as the time when $g(t)$ first reaches the threshold $\vartheta = 6$, and the spike count was given by the total time integral of $G(t)$. These response values were used to find iso-response curves in the same way as in the experiments by searching for combinations $(s_1, s_2)$ that led to the same response. To model iso-response curves recorded under inhibition block, the output of the amacrine cell output was set to zero (Figure 7D, orange line). The scenario with reduced stimulation area (Figure 7D, green line) simply corresponds to a less efficient stimulus, which was modeled by dividing the input into the ganglion cells by a factor of 4, corresponding to a reduction in stimulus area by 75%.

The same model was used to simulate ganglion cell responses to contrast-reversing gratings. Here, the grating stripes had the width of the diameter of the ganglion cell receptive field center and were either aligned to the receptive field or shifted by 90° spatial phase (Supplemental Figure S1). Thus, the two subunits either received the same identical stimulus or were stimulated in antiphase, respectively.


## Supplemental References

Makino, C.L., Taylor, W.R., and Baylor, D.A. (1991). Rapid charge movements and photosensitivity of visual pigments in salamander rods and cones. J Physiol *442*, 761-780.

Perry, R.J., and McNaughton, P.A. (1991). Response properties of cones from the retina of the tiger salamander. J Physiol *433*, 561-587.

Yang, X.L., and Wu, S.M. (1997). Response sensitivity and voltage gain of the rod- and cone-bipolar cell synapses in dark-adapted tiger salamander retina. J Neurophysiol *78*, 2662-2673.